Why vehicle architecture is so important for comfort dynamics? Certain analysis tools of comfort dynamics for vehicle architectures

Jean-Luc Dion, Gwendal Cumunel, Jean-François Rameau

Why vehicle architecture is so important for comfort dynamics ? Certain analysis tools of comfort dynamics for vehicle architectures

Jean-Luc Dion[a], Gwendal Cumunel[b], Jean-François Rameau[c]

[a] *QUARTZ-SUPMECA - Institut Supérieur de Mécanique de Paris / 3 rue Fernand Hainaut / 93400 Saint Ouen / France*
[b] *Université Paris-Est, Laboratoire NAVIER (UMR 8205 CNRS-ENPC-IFSTTAR), Ecole des Ponts ParisTech, 6 et 8 Avenue Blaise Pascal, 77455 Marne-la-Vallée, France*
[c] *Dassault Systèmes / 10 rue Marcel Dassault, CS 40501 / 78946 Vélizy-Villacoublay Cedex / France*

Abstract

Ground vehicle architectures are designed to prevent the transmission of vibration, shock, and noise from the ground profile under operating conditions. The choice of a kinematic architecture strongly contributes to the filtering efficiency of the complete system and has to be considered before the efficiency of the suspension components. In order to highlight the filtering contribution of architectures, all flexible (and dissipative) behaviours are removed in studied models : all the components are assumed as rigid bodies. Thus, this paper focuses on the kinematic filtering performed by ground vehicle architectures, especially articulated suspension systems.
The proposed methodology for studying the filtering efficiency of ground vehicle architectures is described and illustrated by the study of a single wheel to that of the rocker-bogie system used for the rover Curiosity, passing through the intermediate case of a bicycle. Firstly, an original and robust method is proposed in order to simulate this type of mechanism. For this purpose, the kinematics of the studied system is defined by algebraic equations transformed into a set of ordinary differential equations by using an adaptation of the generalized cross product. Secondly, the nonlinear filtering effect of the kinematic function of the system is studied and discussed. This paper provides a set of nonlinear analysis tools applied to kinematics of a ground vehicle, to characterize and analyse architectural designs.
The two main contributions of this work are, first, a kinematic solver method based on generalised cross product, and secondly, dedicated vibration comfort metrics for embedded systems in articulated mechanism (based on nonlinear filtering analysis).

Keywords: Ground vehicles, Wheeled mechanism, Articulated suspension system, Nonlinear filtering, Generalized cross product

Email addresses: jeanluc.dion@supmeca.fr (Jean-Luc Dion), gwendal.cumunel@enpc.fr (Gwendal Cumunel), Jean-Francois.RAMEAU@3ds.com (Jean-François Rameau)

1. Introduction

Tires, dampers and more generally flexible parts in vehicles are designed and optimized in order to ensure the comfort dynamics. Since more than one century, numerous technological innovations have been developed to improve filtering effects in vehicle dynamics. Huge number of researches aims to model, and optimize vibration insulation in order to reduce unsuitable dynamics both for components and passengers. Most of these researches and technological innovation efforts are driven for specific components in a dedicated architecture. This work focuses only on architecture contribution in the vibration suspension. Thus, all flexible parts designed for vibration suspension are removed and all structure components are considered as rigid bodies.
Wheeled systems can induce a smoothing and vibration insulation effects between the ground profile and the wheel center or other specific points of the mechanism. this "pure" kinematics (geometric) effect acts often at the first order before the effects of specific components designed for vibration insulation. For example, in 2013, only few bicycle cross country competitors had 29' wheels but 5 out of the first 6 competitors of the french race "Roc d'Azur" had 29' wheels. During the next year, the larger part of competitors changed their 26' for a 29'. (see [1]). This phenomenon is studied and quantified as a nonlinear filter contributing to the vibration insulation, often in wavelength range larger than that obtained by filtering with components such as dampers. The concepts proposed in this paper are illustrated for different study cases such as a single wheel, a bicycle, and the articulated suspension used for the rover Curiosity.

The mobility system of the rover Curiosity, which is also a suspension architecture, is called rocker-bogie. The rocker-bogie kinematics absorbs most of the vibrations imposed by the ground profile and ensures vibration insulation of the laboratory of the rover Curiosity, located at the top of the rover. This architecture is a convenient example to highlight the efficiency and the robustness of the tools and methods proposed.

As its predecessors, the rover Curiosity is an all-terrain vehicle [2] equipped with a wheeled suspension system [3]. The rocker-bogie system is currently NASA's preferred design for the rover mobility systems [2]. The kinematics of the rocker-bogie system has been studied but few articles have been published about dynamics and the "suspension" aspect of this type of system. The characterization of the phenomenon is not an easy task and several areas of study are possible. Some researchers have studied shocks resulting from an impact between the first wheel and a given geometry placed in its path [4, 5]; others have studied climbing capabilities with experimental tests [6, 7] or minimizing the shaking level at the kinematic center when climbing stairs [5]. An important research theme is also the definition of optimal wheel control to prevent sliding and ensure the stability and efficiency of the mobility system [8, 9].
The study proposed in this article deals with the dynamic behavior, within the meaning of kinematics, of the central point (point L on Figure 1(b)) where the scientific material is attached to the rocker-bogie system (Figure 1(a)). In order to introduce the metric for analyzing the smoothing effect of wheeled systems as well as different representations, simple examples such as a single wheel and a bicycle are also discussed. The goal is to obtain the kinematic filtering function of these nonlinear systems in order to map their filtering capacity according to the parameters of a cosine road profile, i.e. the amplitude and the wavelength.
In this research context two innovative tasks have been driven : an original kinematic solver method based on generalised cross product is developed and dedicated vibration comfort metrics based on nonlinear filtering analysis in articulated mechanism are proposed.

The paper is organized as follows. Section 2 describes the choice of the metric used to analyze and describe the filtering function of wheeled mobility systems. In section 3, a method based on an adaptation of the generalized cross product is presented to generate compact models of wheeled mechanisms. The method is applied to obtain compact kinematic model of some examples (bicycle and rocker-bogie system). Section 4 focuses on the numerical simulations performed for the example of the rover Curiosity on a cosine road profile, especially the problem of bi-contact of the wheels on the ground and initial conditions. Then, a nonlinear filtering analysis of the different systems is provided in section 5. Finally, concluding remarks are discussed.

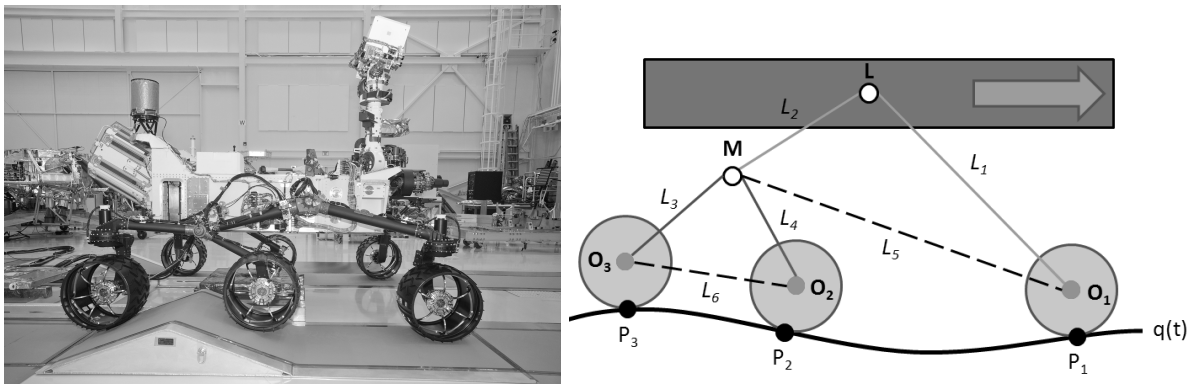

(a) (b)

Figure 1. Rover Curiosity [10] (a) and compact model (b) used in the paper.

2. Filtering efficiency

The smoothing effect performed between the ground profile and the trajectory of the upper point of a mechanism is often an important function of a wheeled system. This function allows smaller amplitudes of motion, behaving as a kinematic insulator, and can thus be considered as a low-pass filter with the ground profile as input and the trajectory of the upper point as output. Like many planar wheeled systems, the relationship between the ground profile and the trajectory of the upper point of the system is strictly algebraic with trigonometric functions and can not be described by a set of Ordinary Differential Equations (ODE) such as for linear filters. Due to the kinematic choices made for an articulated suspension mechanism and the representation of the ground profile, the trajectory of the upper point can be very different and the filter function deeply nonlinear.

In order to describe the filtering efficiency of wheeled mechanisms, a specific ground profile is chosen and filtering efficiency criteria are defined in the two following subsections.

2.1. Excitation choices for nonlinear analysis

In this section, the choice of a ground profile is carried out in order to characterize the system rather than to excite it with a realistic profile, as it can be done with mission replication technique [11]. The choice of the excitation is also performed for the representativeness of the articulated suspension system rather than that of the ground profile.

To analyze the filtering efficiency, four kinds of excitation can be considered [12] (Figure 2) to model the ground profile on which the wheel suspension system moves. The dynamics of the systems is related to the wavelength λ which can also be described as a (space) frequency f or a wave number σ such that:

$$f \equiv \sigma = \left(\frac{1}{\lambda}\right) \tag{1}$$

The first excitation is the step function (Heaviside) described in Figure 2 upper left. This function provides more energy at low frequencies. In the case of a nonlinear low-pass filter, as it can be assumed for the rocker-bogie system, the spectral content of the response consists primarily of low frequencies components, but may also have components in higher frequencies. The main advantage of this type of profile mission is to test the system's ability to overcome obstacles.

The second kind of excitation is random noise that is close to real ground profile, which is one of the main interest of this excitation type (Figure 2 upper right). This excitation is assumed to contain all frequencies at any time. As the Heaviside excitation, due to nonlinearities, the spectral content is mainly contained in low frequencies but higher frequencies can be observed beyond the frequency bandwidth of the random signal.

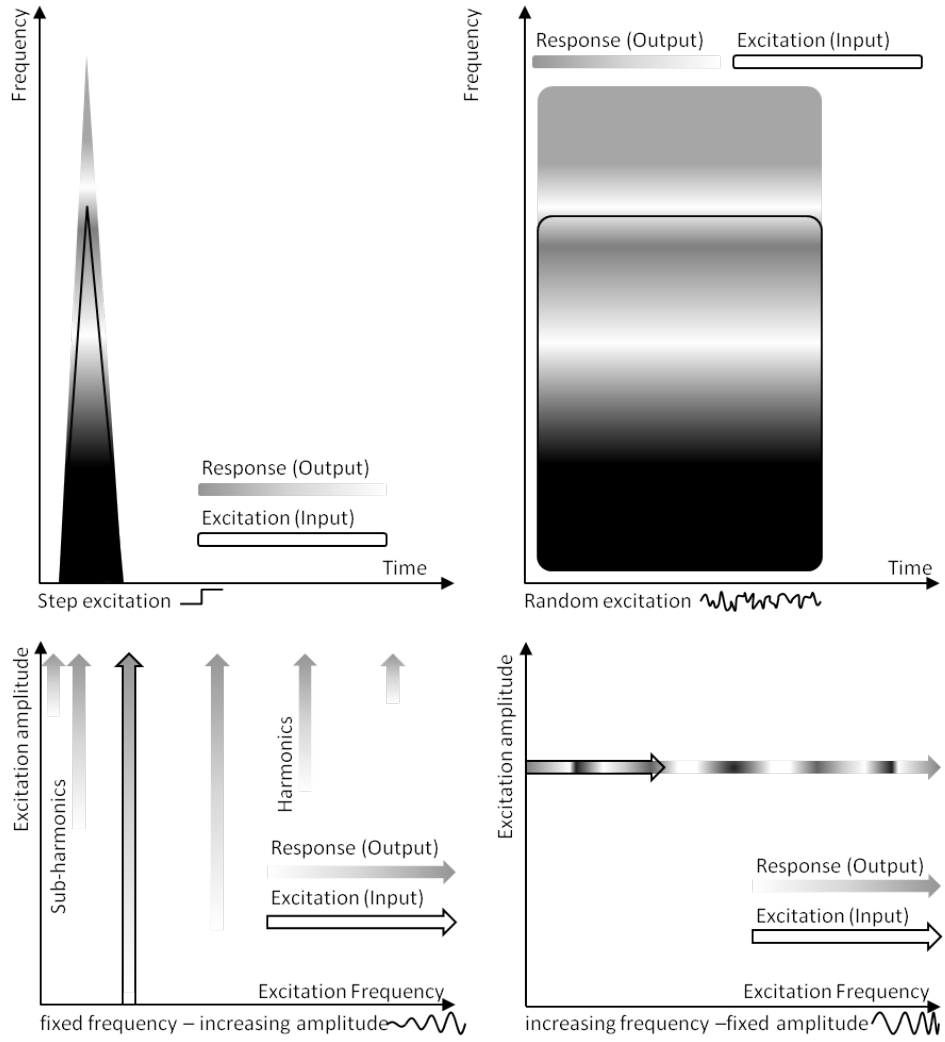

Figure 2. Ground profiles: step (upper left) - random (upper right) - Amplitude Modulated Sine (lower left) - Frequency Modulated Sine (lower right)

Remark : For Heaviside and random noise excitations, all the frequencies are simultaneously represented in the input and in the output. This "frequency mixing" does not allow an accurate and easy characterization of the system and its specific nonlinearities. For this reason, Heaviside and random noise excitations will not be studied in this paper which focuses on the characterization of the filtering effect of articulated suspension systems.

So as to analyze the nonlinearities and the limits of wheeled systems, a sine or cosine excitation is used with amplitude modulations (third case, Figure 2 lower left) or frequency modulations (fourth case, Figure 2 lower right). In these both cases, the excitation is assumed to be slowly modulated. In the third case, i.e. fixed frequency with an increasing amplitude, the observed response is composed of harmonics and, sometimes, of sub-harmonics for specific nonlinearities. For an increasing frequency and a fixed amplitude, the fourth case, the response is also made up of harmonics which move towards higher frequencies when the excitation frequency increases at low frequencies.

Based on these observations and in order to decompose the effect of nonlinearities in the filtering process, we have studied the system under a cosine excitation for different amplitudes and frequencies (or wavelengths).

2.2. Metrics and dynamic filtering efficiency criteria

In order to analyze and optimize the architecture of articulated suspension systems, criteria are defined and based on metric descriptors. The first suggested metric considers the displacement of the upper point of the system, for example the point L for the rover Curiosity (Figure 1 (b)). The proposed measurement $M(t)$, with t the time, is the displacement amplitude normalized to the amplitude of the ground profile:

$$M(t) = \frac{y_L(t)}{2a} \tag{2}$$

with $y_L(t)$ the peak-to-peak vertical displacement of the point L and $2a$ the peak-to-peak displacement amplitude of the ground profile.

This function can be observed in the spectral domain:

$$S\left(\frac{1}{\lambda}\right) = \frac{\mathscr{F}\left(y_L\right)}{2a} \tag{3}$$

with $\mathscr{F}$ the Fourier transform (Discreet Fourier Transform in numerical simulations) and λ the wavelength.

In order to compute compact metrics, two scalar criteria are defined. The first one describes the displacement range regarding the road profile amplitude:

$$C(\lambda, a) = \frac{\mathrm{Max}\left(y_L\right) - \mathrm{Min}\left(y_L\right)}{2a} \tag{4}$$

So as to highlight specific phenomena observed in this study, the second criterion is a spectral criterion based on velocity with respect to the curvilinear abscissa, with s the curvilinear abscissa:

$$C_F(\lambda_0, a) = \frac{\mathscr{F}\left(\frac{\partial y_L}{\partial s}\right)\Big|_{\lambda=\lambda_0}}{2a} \tag{5}$$

Velocity represents a compromise between displacement-based and acceleration-based metrics. Thus, based on the spectral criterion in equation (3), we can also define a spectral criterion using velocity:

$$S_v\left(\frac{1}{\lambda}\right) = \mathscr{F}\left(\frac{\partial y_L}{\partial s}\right) \tag{6}$$

Remark : The criterion $C_F(\lambda_0, a)$ is called "linearized transfer function". These simple criteria allow to point out the efficiency of the mechanism and will be used in section 5.

3. Kinematic compact model based on an adaptation of the generalized cross product

The goal of this section is two folded. On one hand, the traditional three-dimensional cross product is generalized to n dimensions [13]. On the other hand, an ODE is associated to a special class of nonlinear systems by using the generalized cross product. Both are used to set up the compact model.

Remark : this section is develop because we have not found any nonlinear solver able to track certainly complex trajectory in any configurations. Several well known nonlinear solvers (Newton-Raphson method,

tools in Matlab and Python) with several set of parameters have been unsuccessfully assessed.

Let $x_1, \cdots, x_n$ be n vectors of $\mathbb{R}^{n+1}$. By definition, the generalized cross product of $x_1, \cdots, x_n$ is the unique vector $y \in \mathbb{R}^{n+1}$ such that $\det(x_1, \cdots, x_n, z) = \langle y, z \rangle$ for all $z \in \mathbb{R}^{n+1}$, where $\langle \cdot, \cdot \rangle$ denotes the scalar product. Noting $y = \text{Cross}(x_1, \cdots, x_n)$, the i-th coordinate of y is $\det(x_1, \cdots, x_n, e_i)$, where e_i is the i-th canonical vector of $\mathbb{R}^{n+1}$.

$$\text{Cross}(x_1, \cdots, x_n) = \begin{pmatrix} \det(x_1, \cdots, x_n, e_1) \\ \vdots \\ \det(x_1, \cdots, x_n, e_{n+1}) \end{pmatrix} \tag{7}$$

By construction, $\langle x_i, \text{Cross}(x_1, \cdots, x_n) \rangle = 0$ for all $i = 1, \cdots, n$ meaning that the cross product is perpendicular to all its vectors.

Now, this generalized cross product is used to solve a special class of nonlinear systems. Let $F : \mathbb{R}^{n+1} \to \mathbb{R}^n$ be a smooth function, and $X_0 \in \mathbb{R}^{n+1}$ such that $F(X_0) = 0$. The n coordinates of function F are noted

$$F(X) = \begin{pmatrix} f_1(X) \\ \vdots \\ f_n(X) \end{pmatrix} \tag{8}$$

According to differential calculus, if the Jacobian matrix $F'(X_0)$ is full rank, the solution of equation

$$F(X) = 0 \tag{9}$$

in the neighborhood of X_0 is a unique arc of curve $X :]-\varepsilon, \varepsilon[\to \mathbb{R}^{n+1}$ such that $X(0) = X_0$ and $X'(0) \neq 0$. The uniqueness is defined under reparametrization, so that the shape of the curve is unique, not its parametrization. The generalized cross product provides a straightforward way to set up an ODE for computing curve $X(\cdot)$. By hypothesis, $F(X(t)) = 0$ for all $t \in]-\varepsilon, \varepsilon[$, so $\frac{\mathrm{d}}{\mathrm{d}t} F(X(t)) = F'(X(t))X'(t) = 0$ for all $t \in]-\varepsilon, \varepsilon[$, meaning that $X'(t)$ is perpendicular to all gradient vectors $\nabla f_i(X(t))$, $i = 1, \cdots, n$. Then it is necessary and sufficient for $X'(t)$ to be proportional to the cross product of said gradient vectors. Consequently, the vector field $T : \mathbb{R}^{n+1} \to \mathbb{R}^{n+1}$ of the differential equation can be chosen to be the cross product of gradient vectors, that is

$$\begin{aligned} X' &= T(X) \\ X(0) &= X_0 \end{aligned} \tag{10}$$

with

$$T(X) = \text{Cross}(\nabla f_1(X), \cdots \nabla f_n(X)). \tag{11}$$

It should be understood that the differential equation (10) is a pure geometrical feature because it is meaningful under an arbitrary reparametrization. Indeed, considering a reparametrization $Y(t) = X(\varphi(t))$ of solution $X(t)$ such that $\varphi(0) = 0$, it is not difficult to see that $Y(t)$ is also a solution of $F = 0$ because $Y'(t) = \varphi'(t) \cdot \text{Cross}(\nabla f_1(Y(t)), \cdots, \nabla f_n(Y(t)))$ is proportional to the gradients cross product. This fact is worthless to who is only interested in geometry. Furthermore, (10) is useful as long as the vector field (11) does not vanish. In practice, it is enough to check that $T(X_0) \neq 0$ to start the numerical integration, keeping in mind that the numerical solution will not go beyond a point X^* such that $T(X^*) = 0$. It will be seen in the following that the simulations for articulated suspension vehicles does not suffer from these drawbacks.

For example, when $n = 2$ and

$$F(u, v, w) = \begin{pmatrix} g(u, v, w) \\ h(u, v, w) \end{pmatrix}, \tag{12}$$

the three-dimensional curve $t \mapsto (u(t), v(t), w(t))$ such that $F(u(t), v(t), w(t)) = 0$ is the solution of the ODE

$$\begin{pmatrix} u' \\ v' \\ w' \end{pmatrix} = \text{Cross}(\nabla g(u, v, w), \nabla h(u, v, w)) \tag{13}$$

where

$$\text{Cross}(\nabla g, \nabla h) = \begin{pmatrix} \det(\nabla g, \nabla h, e_1) \\ \det(\nabla g, \nabla h, e_2) \\ \det(\nabla g, \nabla h, e_3) \end{pmatrix} = \begin{pmatrix} \begin{pmatrix} g_u & g_v & g_w \\ h_u & h_v & h_w \\ 1 & 0 & 0 \end{pmatrix} \\ \begin{pmatrix} g_u & g_v & g_w \\ h_u & h_v & h_w \\ 0 & 1 & 0 \end{pmatrix} \\ \begin{pmatrix} g_u & g_v & g_w \\ h_u & h_v & h_w \\ 0 & 0 & 1 \end{pmatrix} \end{pmatrix} = \begin{pmatrix} g_v h_w - g_w h_v \\ -(g_u h_w - g_w h_u) \\ g_u h_v - g_v h_u \end{pmatrix} \tag{14}$$

Now, we apply the formulation to different examples (single wheel, bicycle, and rocker-bogie system) by setting up a (9)-like nonlinear system and its associated (10)-like differential equation.

Let $q(\cdot)$ be the parametric planar curve modeling the one dimensional ground (a cosine in our case). Noting r the wheel(s) radius, let $p(\cdot)$ be the parallel curve to curve $q(\cdot)$ at distance r. The contact of radius r wheel(s) with curve $q(\cdot)$ is equivalent to the contact of the wheel(s) center point(s) on curve $p(\cdot)$. This artifact dramatically simplifies the geometry of the problem.

We will now present in detail the case of the rocker-bogie system. The other examples will then be derived from the formulation obtained. The simplified vehicle for the rocker-bogie system includes a rigid triangle together with a constant length line segment articulated at the top vertex of the triangle, as illustrated in Figure 3. For the bicycle, only the rigid triangle will be taken into account and for the single wheel, only the lower left point ($p(u)$). The dimensions of the triangle are lengths l_1, l_2, and angle θ. The length of the articulated line segment is l_3. The unknowns are the three contact points abscissas u, v, w, meaning that the contact points of the simplified vehicle on curve $p(\cdot)$ are $p(u)$, $p(v)$, and $p(w)$. Noting rotation $R(\theta) = \begin{pmatrix} \cos\theta & -\sin\theta \\ \sin\theta & \cos\theta \end{pmatrix}$, with $\theta = \text{acos}\left((l_1^2 + l_2^2 - l_4^2)/(2l_1 l_2)\right)$ where $l_1 = L_6$, $l_2 = L_3$, and $l_4 = L_4$ (Figure 1 (b)), the equations of the problem are:

$$\begin{aligned} &|p(u) - p(v)|^2 - l_1^2 = 0 \\ &|p(u) + \tfrac{l_2}{l_1} R(\theta)(p(v) - p(u)) - p(w)|^2 - l_3^2 = 0. \end{aligned} \tag{15}$$

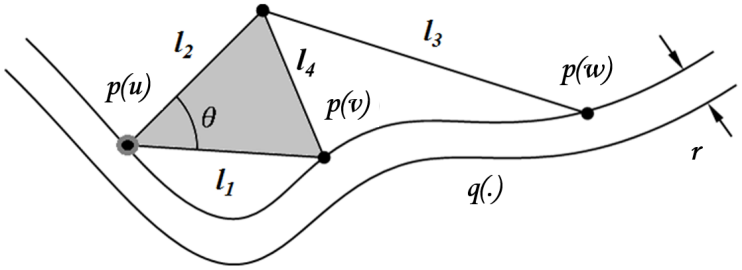

Figure 3. Simple geometric model featuring wheels center points in contact with ground profile offset.

The first equation states that the distance between contact points $p(u)$ and $p(v)$ is length l_1 of the triangle lower segment. The second equation states that the distance between the top vertex $p(u)+\frac{l_2}{l_1}R(\theta)(p(v)-p(u))$ of the triangle and the third contact point $p(w)$ is length l_3 of the articulated line segment.

For numerical solving and simulation purpose, the problem is now changed into an ODE. The first step is to define the solution of (15) as the zero set of a smooth function. Let

$$\begin{array}{l} g(u,v) = |p(u) - p(v)|^2 - l_1^2 \\ h(u,v,w) = |p(u) + \frac{l_2}{l_1} R(\theta)(p(v) - p(u)) - p(w)|^2 - l_3^2. \end{array} \tag{16}$$

Then, let $F : \mathbb{R}^3 \to \mathbb{R}^2$ be the function defined by $F(u,v,w) = (g(u,v), h(u,v,w))$ and (u_0, v_0, w_0) such that $F(u_0, v_0, w_0) = 0$. The nonlinear system

$$F(u,v,w) = 0 \tag{17}$$

is a rewriting of (15) and features one more unknown than equations.

Thanks to the smoothness of function F, and provided matrix $F'(u_0, v_0, w_0)$ is full rank, the solution is a three-dimensional parametrized curve $t \mapsto (u(t), v(t), w(t))$ meaning that $F(u(t), v(t), w(t)) = 0$ for all t in some interval $]-\varepsilon, \varepsilon[$ and $(u(0), v(0), w(0)) = (u_0, v_0, w_0)$. According to previous section, the vector field associated with function F is $T : \mathbb{R}^3 \to \mathbb{R}^3$ defined by

$$T(u,v,w) = \text{Cross}(\nabla g(u,v), \nabla h(u,v,w)) = \text{Cross}\left(\begin{pmatrix} g_u(u,v) \\ g_v(u,v) \\ 0 \end{pmatrix}, \begin{pmatrix} h_u(u,v,w) \\ h_v(u,v,w) \\ h_w(u,v,w) \end{pmatrix} \right). \tag{18}$$

Finally, the ODE turns out to be

$$\begin{array}{l} u' = g_v(u,v) h_w(u,v,w) \\ v' = -g_u(u,v) h_w(u,v,w) \\ w' = g_u(u,v) h_v(u,v,w) - g_v(u,v) h_u(u,v,w) \\ u(0) = u_0 \\ v(0) = v_0 \\ w(0) = w_0 \end{array} \tag{19}$$

with $F(u_0, v_0, w_0) = 0$ and

$$\begin{array}{l} g_u(u,v) = 2 \left\langle p(u) - p(v) \, , \, p'(u) \right\rangle \\ g_v(u,v) = -2 \left\langle p(u) - p(v) \, , \, p'(u) \right\rangle \\ h_u(u,v,w) = 2 \left\langle p(u) + \frac{l_2}{l_1} R(\theta)(p(v) - p(u)) - p(w) \, , \, p'(u) - \frac{l_2}{l_1} R(\theta) p'(u) \right\rangle \\ h_v(u,v,w) = 2 \left\langle p(u) + \frac{l_2}{l_1} R(\theta)(p(v) - p(u)) - p(w) \, , \, \frac{l_2}{l_1} R(\theta) p'(v) \right\rangle \\ h_w(u,v,w) = 2 \left\langle p(u) + \frac{l_2}{l_1} R(\theta)(p(v) - p(u)) - p(w) \, , \, p'(w) \right\rangle \end{array} \tag{20}$$

Remark : equations 19 and 20 represent the core of the solver for the kinematics analysis of multibody systems and is one of the main novelty of this paper.

Furthermore $T(u_0, v_0, w_0) \neq 0$ if matrix $F'(u_0, v_0, w_0)$ is full rank. Then, solving (19) yields the unique solution curve of equation (15) in the neighborhood of (u_0, v_0, w_0), that is the only possible motion of the simplified vehicle. It should be understood that equation (19) captures the geometrical behavior only, as opposed to mechanical or dynamical behavior. In particular, parameter t is a geometrical parameter, it is not the time. The vector field (18) is explicitly computed through partial derivatives of functions g and h.

For the case of the bicycle, in (16), only the first equation is needed, i.e. variable w and function $h(u,v,w)$ do not exist. Thus, the ODE becomes

$$\begin{array}{l} u' = g_v(u,v) \\ v' = -g_u(u,v) \\ u(0) = u_0 \\ v(0) = v_0 \end{array} \tag{21}$$

with $F(u_0, v_0, w_0) = 0$. $g_u(u, v)$ and $g_v(u, v)$ are the same as those defined in (20).

For a single wheel, this procedure is not necessary because the trajectory of the center of the wheel can be obtained analytically.

A large simulation campaign has been performed with several numerical methods. Unlike other tested method commonly used for solving nonlinear system (event detection, conditional solutions, Newton-Raphson algorithm and other tools in Matlab optimization toolbox ®), the proposed method based on the generalized cross product have been used successfully on all studied configurations. Except the proposed method, none of the tested methods allows to simulate the kinematic problem over a large range of wavelength and amplitude. Problems encountered with previous methods are due to non convergent solutions, periodic solutions that do not move the rover forward, non continuous solutions and solutions that did not respect the defined architecture design in specific step of the simulation.

4. Numerical simulations

In order to perform numerical simulations, we first estimate the dimensions of the rover Curiosity for the compact model. Thus the dimensions in pixels are extracted from a photo (Figure 4).

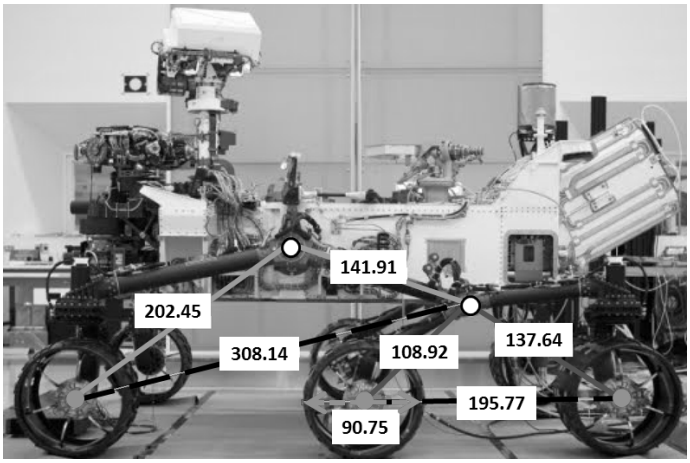

Figure 4. Estimation of the rover dimensions for numerical simulations (lengths are in pixels) - NASA picture [14].

As the diameter of the wheels is known, equal to 0.5 m, the conversion coefficient from pixels to meters is deduced (1/181.5). The Table 1 lists the dimensions taken for the compact model.

Table 1
Dimensions used for the rover Curiosity.

L_i	1	2	3 ($=l_2$)	4	5 ($=l_3$)	6 ($=l_1$)	$2r$
Length (in pixels)	202.45	141.91	137.04	108.92	308.14	195.77	**90.75**
Length (in m)	1.12	0.78	0.76	0.60	1.70	1.08	**0.5**

For the bicycle, the dimensions of a commercial MTB were chosen (Tab. 2).

Table 2
Dimensions used for the bicycle.

L_6 ($=l_1$) (m)	L_3 ($=l_2$) (m)	θ (rad)	$2r$
1.23	0.67	1.15	0.5

The numerical simulations are done for a cosine road profile defined by $q(t) = a\cos\left(\frac{2\pi}{\lambda}t\right)$. The cosine profile is chosen instead of the sinusoidal one for practical convenience to access initial conditions (position of the rover on the road profile). With this profile, the initial position of the center of the back wheel is easy to determine and is equal to $[0\ a+r]$. However, the results will have been exactly the same with a sinusoidal road profile. In the following of the article, the road profile type will be abusively called sinusoidal.

4.1. Application of the compact model to a sinusoidal road profile

Let $M(t)$ a point of the road profile defined by $\overrightarrow{OM}(t)=[t\ q(t)]$ (Figure 5). Then, for the point $P(t)$ representing the wheel center(s) trajectory, we have $\overrightarrow{OP}(t) = \overrightarrow{OM}(t) + r\vec{n}(t)$ where $\vec{n}(t)$ is the normal unit vector of the Frenet-Serret frame. The normal unit vector is defined by

$$\vec{n}(t) = \frac{1}{\sqrt{1+q'(t)^2}} \begin{bmatrix} -q'(t) \\ 1 \end{bmatrix} \tag{22}$$

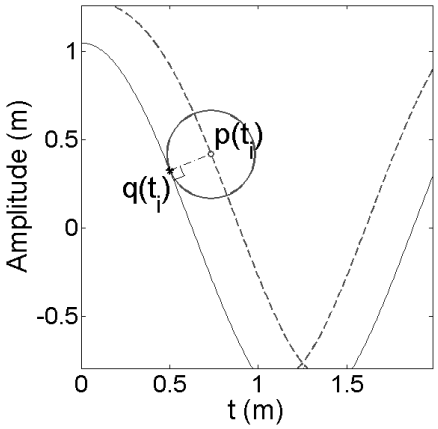

Figure 5. Wheel center trajectory on a cosine road profile.

So the function $p(t)$ describing the trajectory of the wheel center(s) is obtained

$$p(t) : \begin{cases} x(t) = t - \frac{rq'(t)}{\sqrt{1+q'(t)^2}} \\ y(t) = q(t) + \frac{r}{\sqrt{1+q'(t)^2}} \end{cases} \tag{23}$$

Then, this function is used in equation (19) to provide a solution for the rover Curiosity kinematics (with rigid bodies) on a sinusoidal road profile.

4.2. "Bi-contact" case

We choose arbitrarily to study the compact model for a=$[r/2\ 10r]$ m and λ=$[2r\ 10r]$ m. With these parameter ranges, the curvature radius of the road profile can be inferior to the radius of the wheels. Thus we have to deal with "bi-contact" phenomenon, called afterward Bicontact. Bicontact occurs when the wheel is in contact with two lobes of the sinusoidal profile.

The curvature radius R_c of a curve $q(t)$ is defined by

$$R_c = \frac{(1+q'(t)^2)^{3/2}}{q''(t)} \tag{24}$$

In our case, we have $q(t) = a\cos(2\pi t/\lambda)$, so

$$R_c(a,\lambda) = -\frac{\left[\lambda^2 + 4\pi^2 a^2 \sin^2\left(\frac{2\pi}{\lambda}t\right)\right]^{3/2}}{4\pi^2 a\lambda\cos\left(\frac{2\pi}{\lambda}t\right)} \tag{25}$$

The minimum of the absolute value of the curvature radius for the cosine road profile, $R_c^{\min}$, is attained for $t = \pm k\,\frac{\lambda}{2}$ with k$\in \mathbb{N}$. It leads to

$$R_c^{\min}(a,\lambda) = \frac{\lambda^2}{4\pi^2 a} \tag{26}$$

The condition to have Bicontact in numerical simulations is

$$R_c^{\min}(a,\lambda) < r \Leftrightarrow \frac{\lambda^2}{4\pi^2 r} < a \tag{27}$$

Thus in the (λ, a)-plane, the equation of the limit curve delimiting where Bicontact occurs is $a = \frac{1}{4\pi^2 r}\lambda^2$. The Figure 6 shows that, for the parameter ranges chosen, the Bicontact area is very large compared to that without Bicontact. The points (a), (b), and (c) correspond to cases depicted in Figure 7.

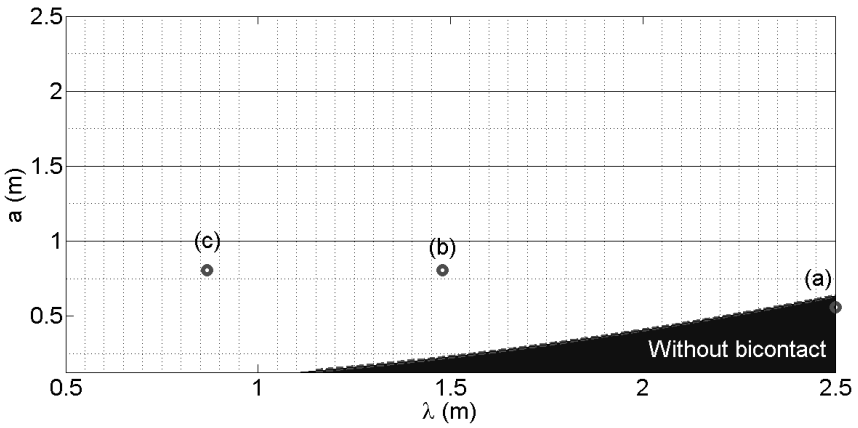

Figure 6. Bicontact zone for the numerical simulations with $a \in [r/2\ 10r]$ m and $\lambda \in [2r\ 10r]$ m.

The Figure 7 illustrates some cases of the parameters domain with, (a), and without, (b)(c), Bicontact. The dotted curves represent the wheel center trajectories. For the Bicontact cases, the bold line is the useful part of the wheel center trajectory. The part of the curve between the two points is not traveled by the contact point of the wheel. The lower the absolute value of the radius of curvature is smaller than the radius of the wheel, the larger the unused part of the profile curve.

Bicontact is not a crucial point in the numerical simulations for most couples of parameters (a, λ) because, as the function $p(t)$ defined in equation (23) is C^∞, there is no discontinuity in solving the system (19). The simulation points for which the wheel centers are in the Bicontact loops can be removed after the calculation. On a standard laptop with the same solver parameters, for a=0.804 m and λ=0.867 m (Figure 7(c)), the computational times with and without Bicontact are respectively 2.42 s and 5.50 s. There is not a big difference for one simulation case however to map the filtering efficiency of the rocker-bogie system, with a good accuracy (for example a discretization of 50 by 50), the gain of computational time is much more important. Thus Bicontact is important as regards the computational time and also the accuracy of the results for pairs of parameters (a, λ) where the wheel radius is substantially greater than the minimum of the absolute value of the curvature radius. The problem is that, for these cases, a significant part of the computational time is spent on a part of the curve that does not interest us. Moreover, another drawback is that the accuracy on the interest part of the curve decreases because less points are obtained for this useful part of the curve.

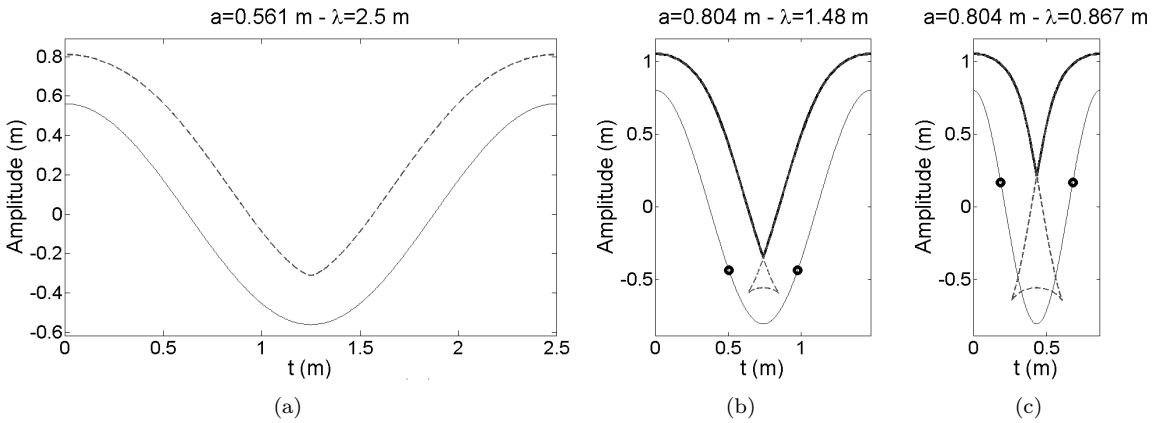

Figure 7. Bicontact for different values of a and λ: (a) a=0.561 m and λ=2.5 m, (b) a=0.804 m and λ=1.48 m, and (c) a=0.804 m and λ=0.867 m.

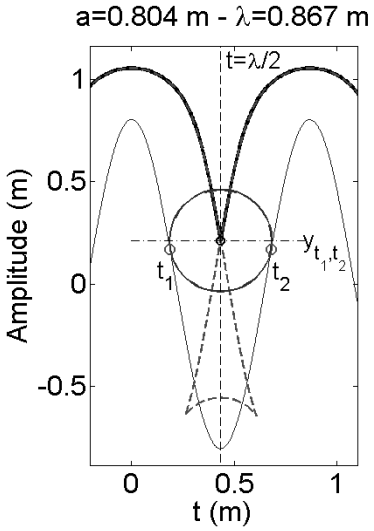

Figure 8. Bicontact scheme for numerical simulations

With a cosine road profile, it is obvious that the self-intersection point abscissa is equal to $\lambda/2$. Thus with equation (23), in order to find the two curvilinear abscissas t_1 and t_2 of the road profile, corresponding to the self-intersection point of the wheel center trajectory at $t = \lambda/2$, one have to solve:

$$\left(t - \frac{\lambda}{2}\right)^2 = \frac{r^2\, q'(t)^2}{[1 + q'(t)^2]^2} \tag{28}$$

Then, the height y_{t_1,t_2} can be established

$$y_{t_1,t_2} = p(t_1 \text{ or } t_2) = q(t_1 \text{ or } t_2) + \frac{r}{\sqrt{1 + q'(t_1 \text{ or } t_2)^2}} \tag{29}$$

4.3. Initial conditions

Another aspect that must be taken into account for the simulation, particularly for the computational time, is the initial conditions, i.e. the initial configuration of the compact model on the cosine road profile.

As previously said, the solution arc is unique. Therefore only one initial configuration of the rover, from all those possible, allows to succeed in finishing the numerical simulation for a given amplitude and a given wavelength of the road profile. So a specific procedure has to be established. This is also the case for the simulations on the bicycle, but to a lesser extent.

The Figure 9 presents the five possible initial configurations for cosine profile parameters a=0.804 m and λ=1.357 m. The values of the contact points $u_0(= u(0))$, $v_0(= v(0))$, and $w_0(= w(0))$ are given in Table 3 for the different initial configurations. The trajectories of the the point L (parametrized curve of $y_L(t)$ versus $x_L(t)$) for the five configurations are illustrated on Figure 10.

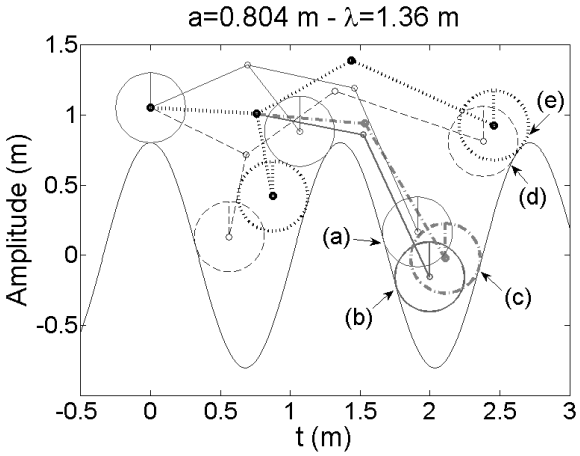

Figure 9. Initial conditions of the compact model for cosine profile with parameters a=0.804 m and λ=1.357 m.

Table 3
Contact point abscissas for the different initial conditions for cosine profile parameters a=0.804 m and λ=1.357 m

Initial configuration	u_0 (m)	v_0 (m)	w_0 (m)
(a)	0	0.32	2.60
(b)	0	1.12	1.76
(c)	0	1.12	2.35
(d)	0	1.12	2.65
(e)	0	1.27	1.67

For the cosine profile presented in Figure 10, all the simulations with the different initial conditions have finished ($u(t) = \lambda$). The solutions obtained for the different configurations are a part of the same parametrized curve with different starting points on the curve depending on the initial condition. The initial configuration leading to a full period ($y_L(0) = y_L(T)$) is the configuration (d) (Figure 10).

However, in other cases, we can have "circular" solutions because the condition to finish the simulation ($u(t) = \lambda$) is never attained. The Figure 11 shows an illustration of three different initial positions for road profile parameters a=0.804 m and λ=1.071 m. For this case, there are five initial conditions possible. Two solutions lead to the circular solution n°2, two others to the circular solution n°3, and only one to the "full-period" solution n°1.

For the numerical results presented in the next section, each parameter ranges a=[r/2 10r] m and λ=[2r 10r] m were discretized in 50 points, resulting in 50×50 cases for the mesh of the studied domain.

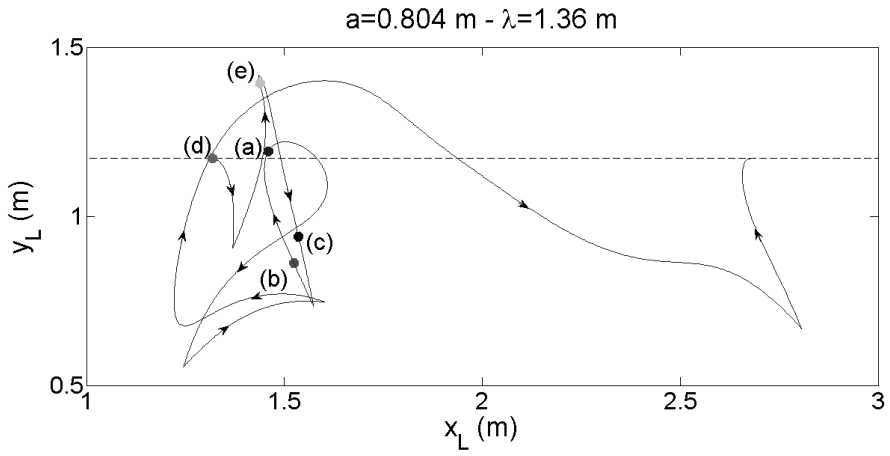

Figure 10. Point L trajectory ($y_L = f(x_L)$) for different initial conditions of the compact model for cosine profile parameters a=0.804 m and λ=1.357 m.

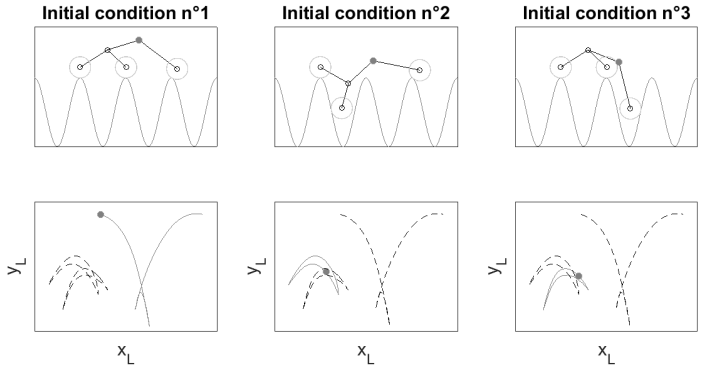

Figure 11. Animation example with different initial conditions for road profile parameters a=0.804 m and λ=1.071 m. The initial conditions n°2 and 3 leads to circular solutions.

5. Nonlinear filtering analysis

The metrics defined in section 2.2 are used in this section to highlight the efficiency, main properties, and some limitations of wheeled mechanisms. In the first part, the analysis of a global criteria is carried out only for the cases of the bicycle and rocker-bogie system, because the single wheel case is not of particular interest. Then, in a second part, a harmonic analysis on the three systems is presented.

5.1. Global criteria analysis

In order to normalize wavelengths and amplitudes, both variables are divided by the distance L_6 (between the wheels $n°2$ (O_2) and $n°3$ (O_3), in Figure 1(b)) for the rocker-bogie system and the bicycle. As a consequence, all following figures are built with dimensionless variables.

The first mapping of the filtering efficiency (Figure 12 for the bicycle and Figure 13 for the rocker-bogie system) depicts the ratio between the vertical displacement of the point L and the amplitude a of the ground profile, $C(\lambda, a)$ defined in equation (4).

This metric is based on a nonlinear criterion (peak-to-peak amplitude) and shows the efficiency of the rocker-bogie architecture to filter high frequencies (i.e. short wavelength - see points (s) on Figures 12 to 15) and small amplitudes. However, when the wavelength is close to the distance between the centers of the wheels

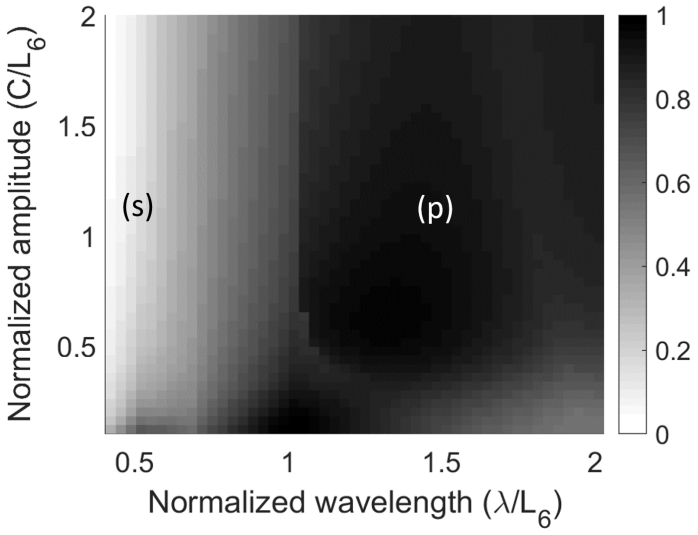

Figure 12. Mapping of the filtering effect of a bicycle based on the displacement amplitude criterion $C(\lambda, a)$, normalized to the distance between wheels. A good efficiency for wavelengths smaller than spacing between wheels is observed.

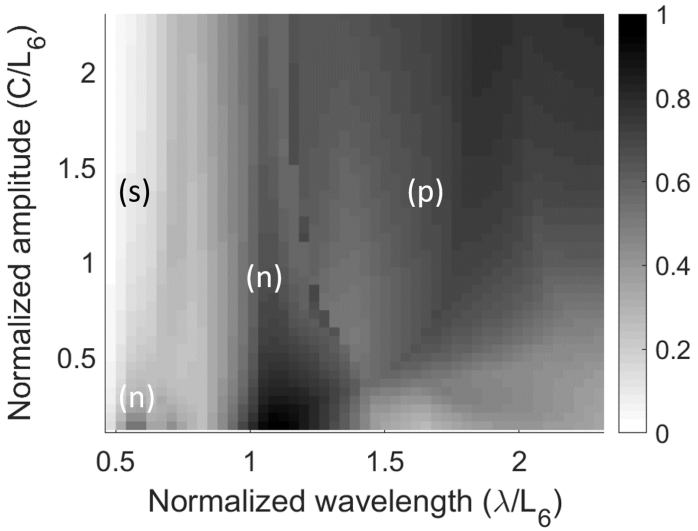

Figure 13. Mapping of the filtering effect of the rocker-bogie system based on the displacement amplitude criterion $C(\lambda, a)$, normalized to the distance between wheels. The filtering effect of the rocker-bogie architecture is globally better than that of the bicycle. Nonlinearities depending on high amplitudes are greater than those observed for the bicycle.

($n°2$ and $n°3$ for the rocker-bogie system), the amplitude of the point L is not reduced anymore compare to the ground profile amplitude (see points (n) on Figures 12 to 15).

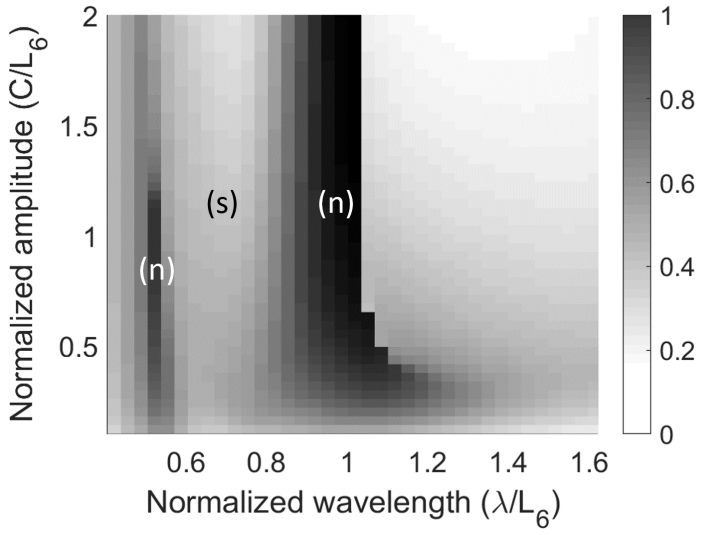

Figure 14. Mapping of the linearized transfer function for the bicycle, built with the vertical displacement amplitude that occurs at the excitation wavelength induced by the ground profile ($C_F(\lambda_0, a)$, equation (5)). The bicycle architecture behaves like an efficient filter except for wavelengths close to the spacing between wheels or its half (points (n)), for which a poor efficiency in the kinematic filtering is observed.

Another way to analyze the frequency filtering is to represent the linearized transfer function between the ground profile and the wheeled system, $C_F(\lambda_0, a)$ defined in equation (5). This transfer function is computed as the ratio between the response and the excitation at the fundamental frequency (of the excitation) and is depicted in Figure 14 for the bicycle and Figure 15 for the rocker-bogie system.

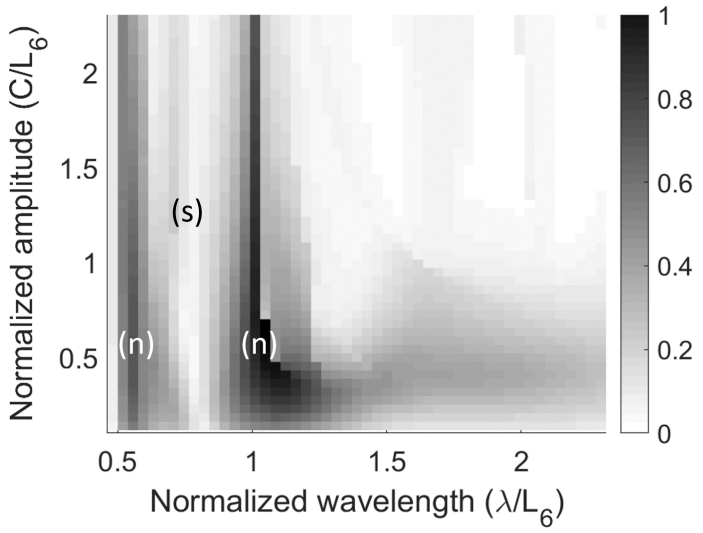

Figure 15. Mapping of the linearized transfer function for the rocker-bogie system, built with the vertical displacement amplitude that occurs at the excitation wavelength induced by the ground profile ($C_F(\lambda_0, a)$, equation (5)). The rocker-bogie architecture behaves also like an efficient filter except for wavelengths close to the spacing between wheels or its half (points (n)), for which a poor efficiency in the kinematic filtering is observed (see Figure 16).The system is more efficient than a simple bicycle but highlights more complex nonlinearities.

Remark : For most of the mechanisms designed for vibration insulation, the use of wheels and kinematic joints leads to dynamics that can be observed as a low-pass filter, in a global point of view. Such mechanisms are mainly effective for wavelengths close to or smaller than the main dimensions of the mechanism (wheelbase for example, points (s) on Figures 12 to 15).

The bicycle and rocker-bogie architectures, observed as linear filters, behaves like an efficient filter. The band-stop (points (s) on Figures 12 to 15) applies for short wavelengths, smaller than the spacing between wheels (high frequencies), and the band-pass (points (p) on Figures 12 to 13) for large wavelengths. This architecture solution fits globally to the vibration insulation needs. This kinematic filtering effect is the main reason that leads mountain bike manufacturers to choose larger wheels in the last decade (from 26' to 29') and to remove rear suspension, see [1].

Remark : By comparing the bicycle (Figure 12) and the rocker-bogie (Figure 13) architectures, we can observe that the more the architecture of the wheeled system is complex, greater is the efficiency of the kinematic filtering, as well as the nonlinearities.

However, for specific wavelengths close or equal to the spacing between the wheels or its half (points (n) on Figures 13 to 15), the kinematic filtering does not work so much (see example in Figure 16).

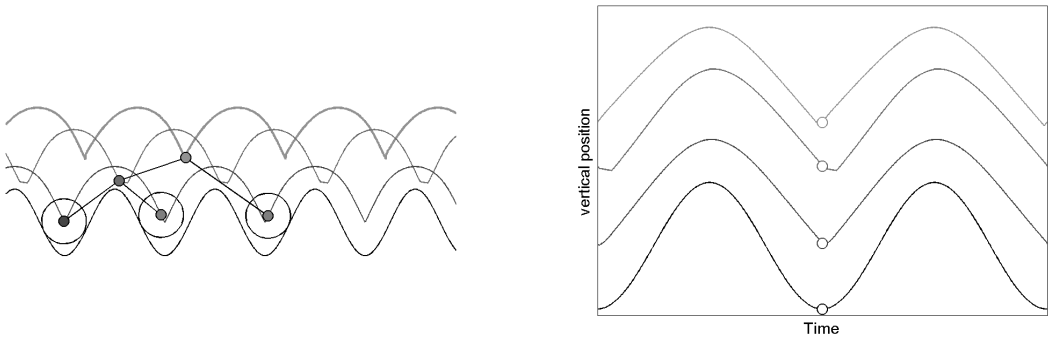

Figure 16. Kinematics of the rocker-bogie system for ground wavelength close to the spacing between wheels.

5.2. Harmonic analysis

Larger is the amplitude and more complex is the motion, up to configurations (unrealistic) such as the one depicted in Figure 17.

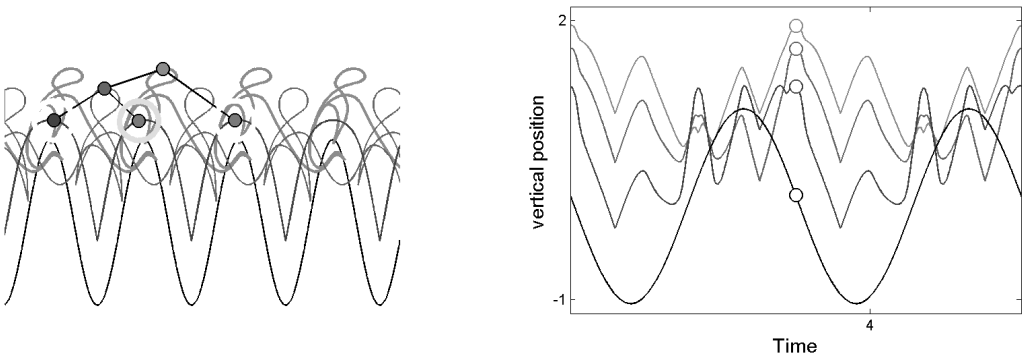

Figure 17. Example of complex kinematics obtained for the rocker-bogie system.

The fundamental transfer function of the rocker-bogie system (Figure 15) reveals a good filter efficiency. However, this efficiency only concerns the response of the point L at the excitation wavelength of the ground

profile. In fact, the periodic motions are complex and far from a sinusoidal signal (see left side of Figure 17). The spectral content is rich in high frequencies: the kinematic system is strongly nonlinear. More the amplitude increases, more the nonlinearity is exhibited, and more the high frequencies spectral domain is energetic. In order to emphasize this fact, two kinds of graphs are depicted in Figures 18 to 20. On the upper graph, the spectral content is plotted for a given amplitude of the road profile versus the harmonic order (horizontal axis) and the normalized wavelength (vertical axis). The order (normalized frequency) represents the number of events per period. On the lower graph, the spectral content is plotted for a given amplitude of the road profile versus the harmonic order (horizontal axis) and the amplitude of each harmonic (vertical axis). The gray level on the lower graph represents the evolution of harmonics versus wavelength, from the white (0.5 m) to the black (2.5 m).

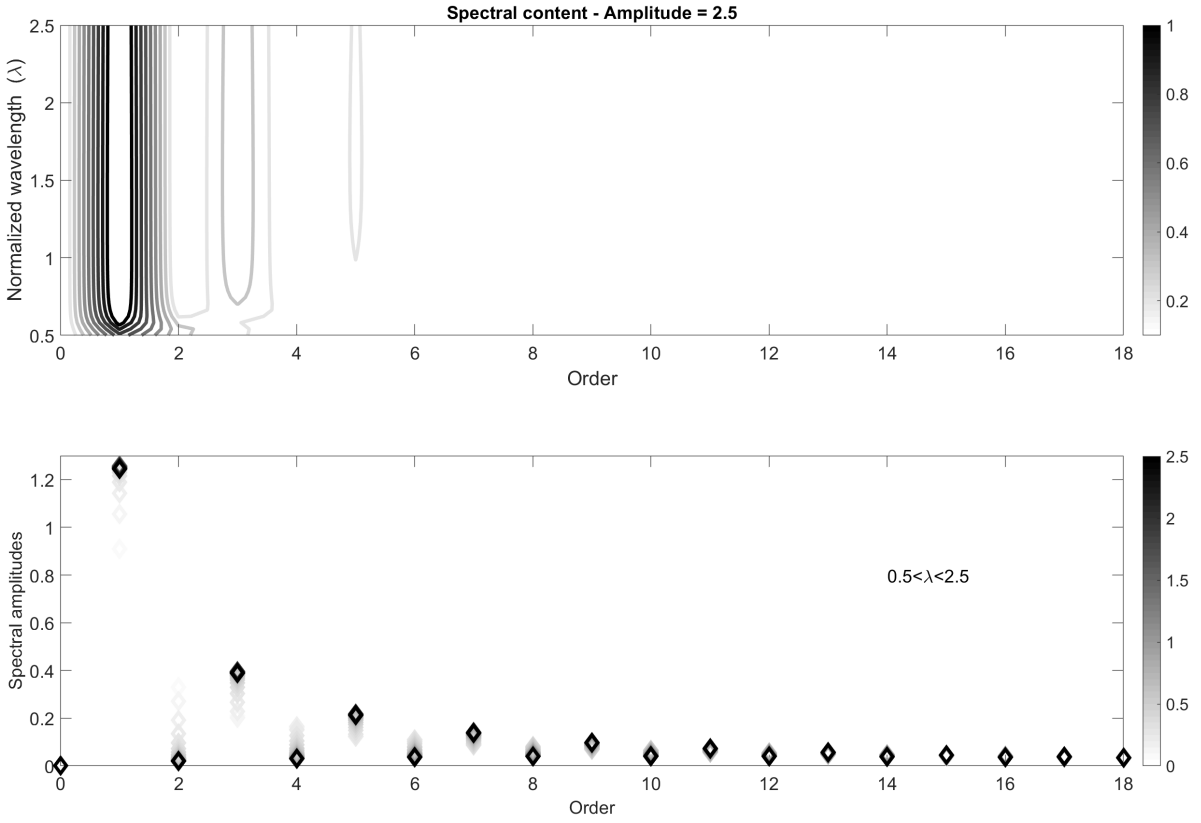

Figure 18. Spectral content versus wavelengths and amplitudes ($S_v(1/\lambda)$ in equation (6)) for a single wheel: the natural kinematic filtering induces a nonlinear behavior with odd harmonics.

In that way, the evolution of the spectral content versus the amplitude and normalized wavelength of the road profile is depicted in Figure 18 for a single wheel, Figure 19 for a bicycle, and Figure 20 for the rocker-bogie system.

For low amplitudes (see left part of Figure 20), a wheeled system acts like a linear one: the response occurs mainly at the excitation frequency. When the amplitude increases (see Figure 18, Figure 19, and right part of Figure 20), the spectral content switches to higher frequencies, mostly to the second harmonic for the bicycle and to the third harmonic for the rocker-bogie system, and the amplitude of the fundamental frequency tends to be low. The evolution of the frequency content are quite simple for a single wheel (Figure 18), becomes more complex for a bicycle (Figure 19), and very rich for the rocker-bogie architecture as show

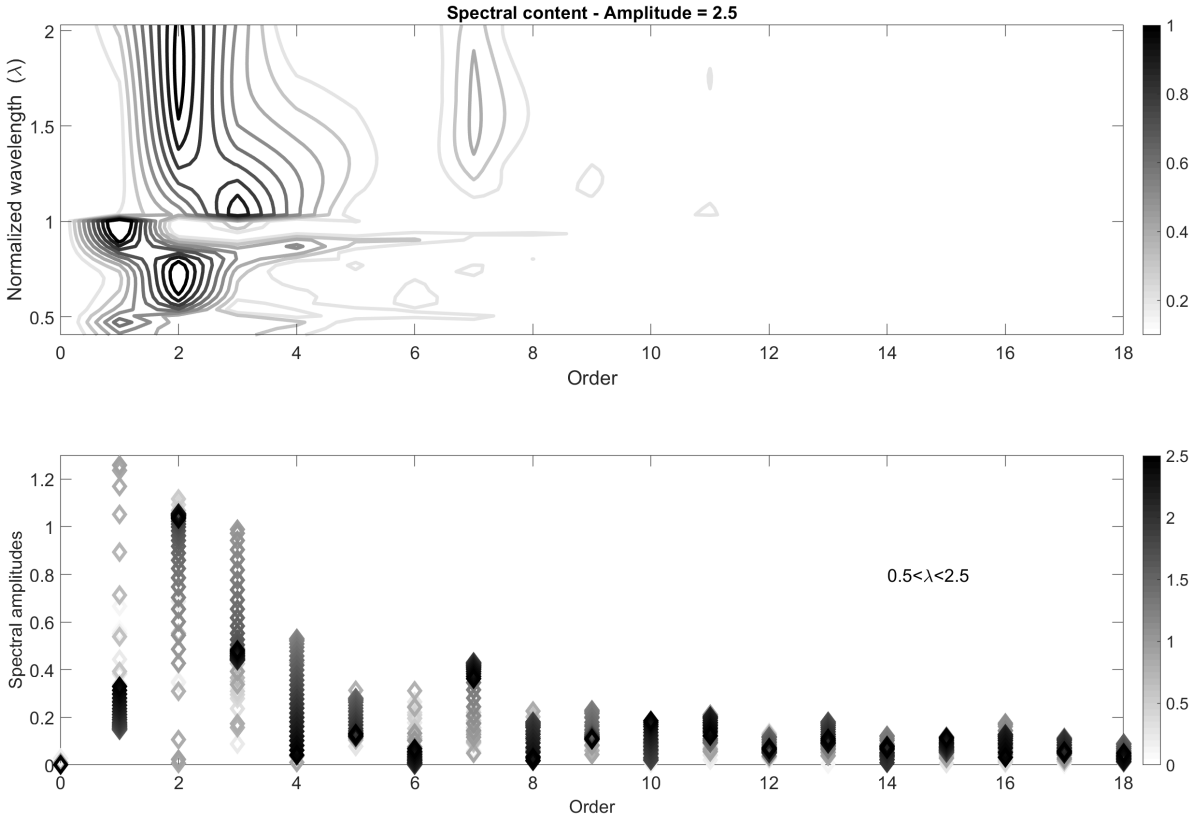

Figure 19. Spectral content versus wavelengths and amplitudes ($S_v(1/\lambda)$ in equation (6)) for a double wheeled system (bicycle): the filtering effect combines the effect of a single wheel and the distance between wheels. The system is clearly efficient except for wavelengths equal to the distance between wheel and its half.

in the Figure 20.

Remark : This spectral point of view confirms that the complexity of the architecture allows a better filtering efficiency but induces important nonlinearities and high frequencies content.

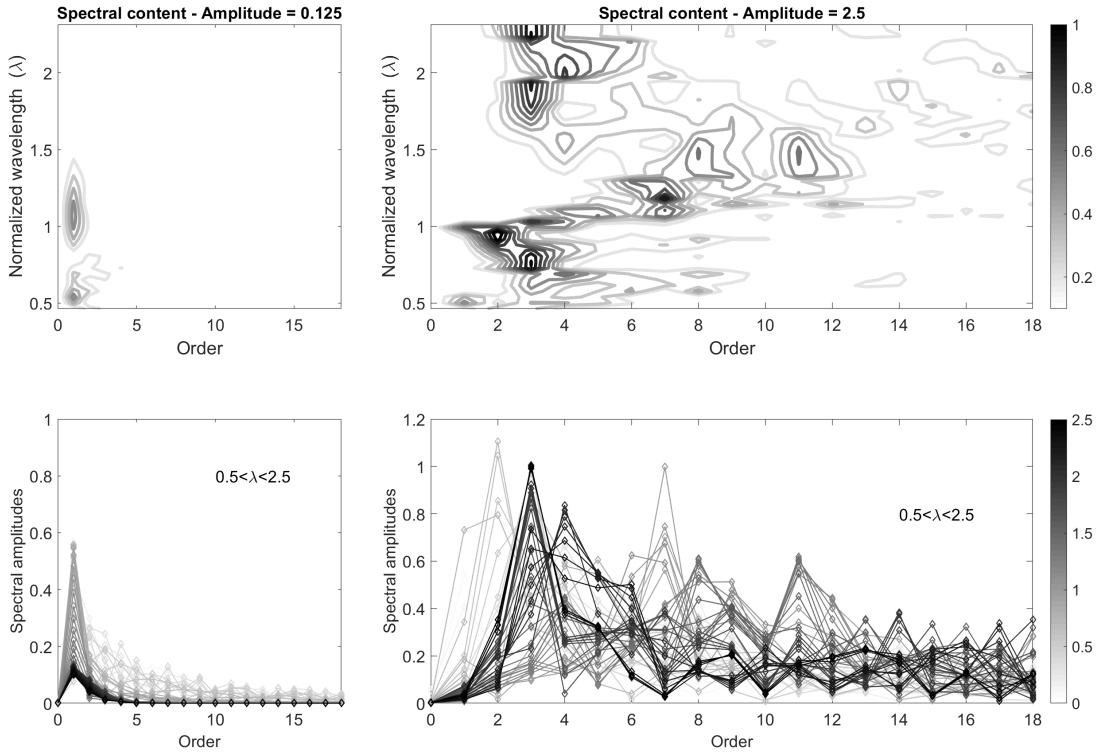

Figure 20. Spectral content versus wavelengths and amplitudes ($S_v(1/\lambda)$ in equation (6)) for the rocker-bogie system: for small amplitudes (left part) the system acts as a linear system without harmonic content; when the amplitude increases (right part), nonlinearities introduce harmonics and the spectral energy goes to higher frequencies domain.

6. Conclusion

Vibration insulation for large amplitudes is often achieved with multibody kinematics, such as Steadicam system or bike suspension, for example. In this article, the vibration insulation performed by wheeled system architectures is studied and observed as a nonlinear filter induced by kinematics.

In order to describe the filtering efficiency of wheeled mechanisms, a specific ground profile is chosen and filtering efficiency criteria are defined. So as to analyze the nonlinearities and the limits of wheeled systems, a cosine excitation is used with amplitude or frequency modulations. This excitation type allows an accurate characterization of the efficiency of vibration insulation. Using the generalized cross product, we proposed to transform the complete set of algebraic equations describing kinematics of a wheeled mechanism (which could not be solved by classical non linear solvers) into an original set of ordinary differential equations, leading to a compact formulation of a wheeled system easy to solved. To illustrate this formulation, three systems have been studied with a progressive complexity: from a single wheel up to the rocker-bogie system, passing through a bicycle. Parallel robots like the rover Curiosity, with the rocker-bogie suspension, are very good candidates for vibration insulation.

The main effect of wheeled system architectures depicted in this study is the transfer of energy from low frequencies to high frequencies. The complexity of the wheeled system architecture induces a better filtering efficiency on a larger bandwidth but also important nonlinearities that transfer energy in high frequencies domain. This phenomenon is induced by kinematics nonlinearities such as rotations. The energy which can be concentrated in a narrow bandwidth with high levels in low frequencies is transferred in high frequencies

with lower levels and in larger bandwidths. In real systems, this high frequencies energy is attenuated with secondary mechanisms, such as tires, dampers, bodies flexibility and joints with viscoelasticity or friction and more generally with dissipative effects. The main contribution in vibration insulation of such architectures is not to dissipate the energy but to transfer it in higher frequencies domain with lower levels.

The proposed vibration filter efficiency tool highlights some lacks in the current architecture of the rocker-bogie system that could be pushed over with a design optimization. The tools described in the article are easy to develop and compute. In that way, they are convenient for optimizing at the first order the design parameters of vehicle architectures for wheeled mechanisms to improve their insulation performance against vibrations.

Bibliography

References

[1] Thomas Steiner, Beat Müller, Thomas Maier, and Jon Peter Wehrlin. Performance differences when using 26- and 29-inch-wheel bikes in swiss national team cross-country mountain bikers. *Journal of Sports Sciences*, 34(15):1438–1444, 2016.

[2] B.D. Harrington and C. Voorhees. The challenges of designing the rocker-bogie suspension for the mars exploration rover. In *37th Aerospace Mechanisms Symposium*, NASA Johnson Space Center, May 2004.

[3] J. Lin and A.A. Goldenberg. Development of a terrain adaptive mobile robot and its application in space exploration. *Recent Patents on Space Technology*, 1(2):167–179, 2011.

[4] D.P. Miller and T.-L. Lee. High-speed traversal of rough terrain using a rocker-bogie mobility system. In *Space 2002 and Robotics 2002: Eighth International Conference on Engineering, Construction, Operations, and Business in Space*, pages 428–434. ACSE Library, 2002.

[5] D. Kim, H. Hong, H.S. Kim, and J. Kim. Optimal design and kinetic analysis of a stair-climbing mobile robot with rocker-bogie mechanism. *Mechanism and machine theory*, 50:90–108, 2012.

[6] T.-L. Lee. Behavior and control of a rocker-bogie suspension under relatively high speed. Master's thesis, University of Oklahoma, USA, 2002.

[7] R.A. Lindemann and C.J. Voorhees. Mars exploration rover mobility assembly design, test and performance. In *International Conference on Systems, Man and Cybernetics*, volume 1, pages 450–455. IEEE, 2005.

[8] T.M. Howard and A. Kelly. Optimal rough terrain trajectory generation for wheeled mobile robots. *The International Journal of Robotics Research*, 26(2):141–166, 2007.

[9] D.M. Helmick, Y. Cheng, D. Clouse, M. Bajracharya, L.H. Matthies, and S.I. Roumeliotis. Slip compensation for a mars rover. In *International Conference on Intelligent Robots and Systems*, pages 2806–2813. IEEE, 2005.

[10] NASA/JPL-Caltech. Mars rover curiosity, right side view, 2011.

[11] Alexander Steinwolf. Random vibration testing beyond psd limitations. *Sound and Vibration*, 40(9):12–21, 2006.

[12] J.-L. Dion, G. Chevallier, and N. Peyret. Improvement of measurement techniques for damping induced by micro-sliding. *Mechanical Systems and Signal Processing*, 34(1-2):106–115, 2012.

[13] S. Doplicher and J.E. Roberts. Endomorphisms of c*-algebras, cross products and duality for compact groups. *Annals of Mathematics*, 130(1):75–119, 1989.

[14] NASA/JPL-Caltech. Nasa's curiosity rover in profile, 2011.